Gradual spin crossover behavior encompassing room temperature in an Iron(II) complex based on heteroscorpionate ligand

Oleksandr Ye. Horniichuk, Laure Vendier, Lionel Salmon,* Azzedine Bousseksou*

LCC, CNRS and Université de Toulouse (UPS, INP) 205 route de Narbonne, F-31077 Toulouse, France.

Figure S1: Crystal structure of the product formed in an attempt of reduction of $^{n}Bu_4NL^1$. Hydrogen atoms are omitted for clarity. Displacement ellipsoids are drawn at 50% probability level.

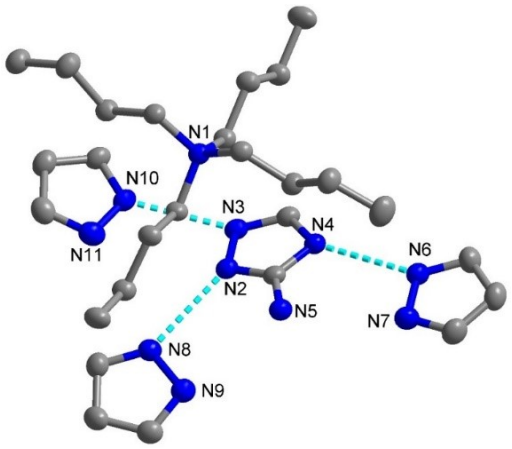

Figure S2: ^{1}H NMR spectrum (aromatic region) of product obtained in an attempt to reduce $^{n}Bu_4NL^1$ (solvent – CD_3OD).

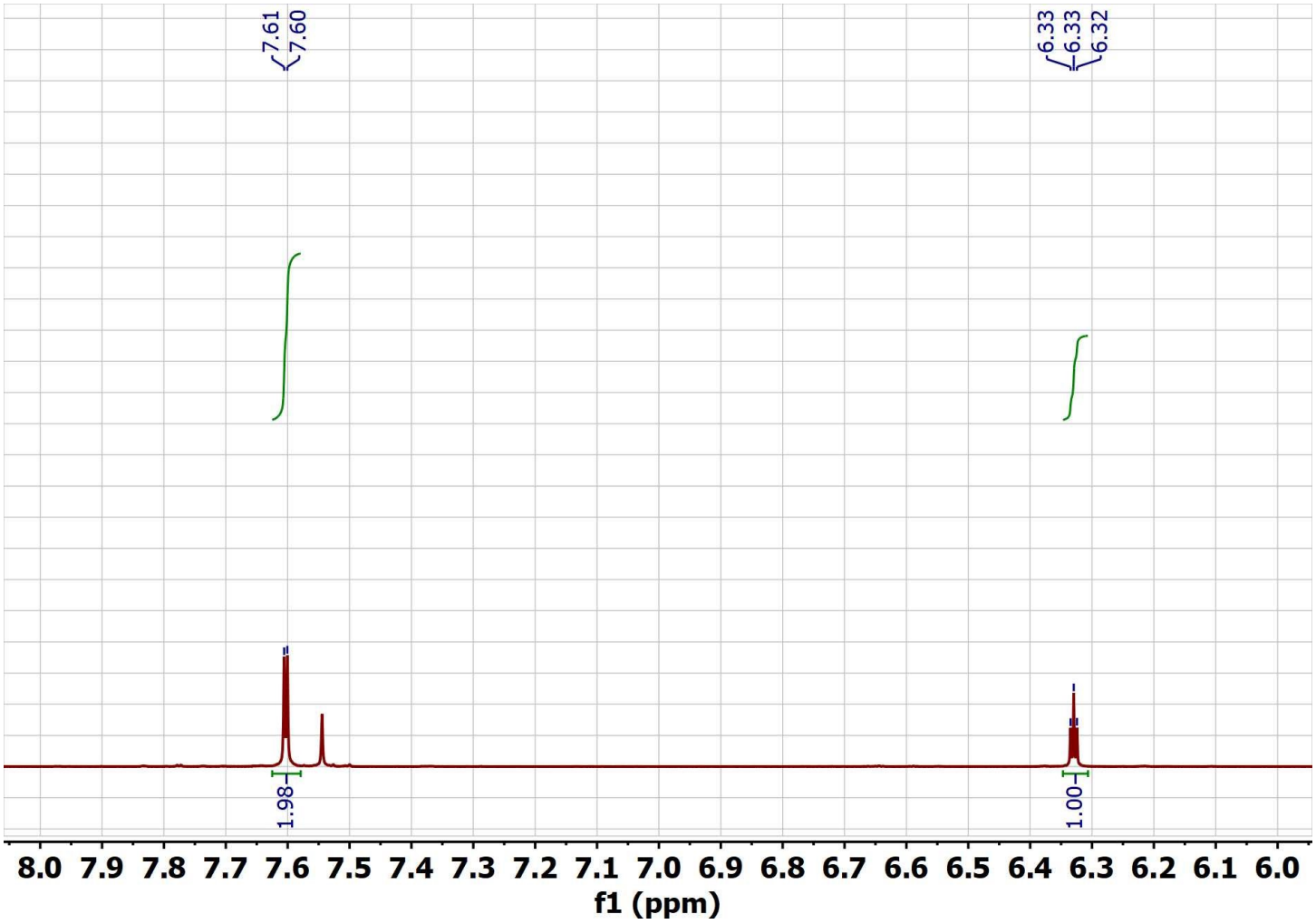

Figure S3: ^{1}H NMR spectrum (aromatic region) of $^{n}Bu_4NL^1$ in CD_2Cl_2.

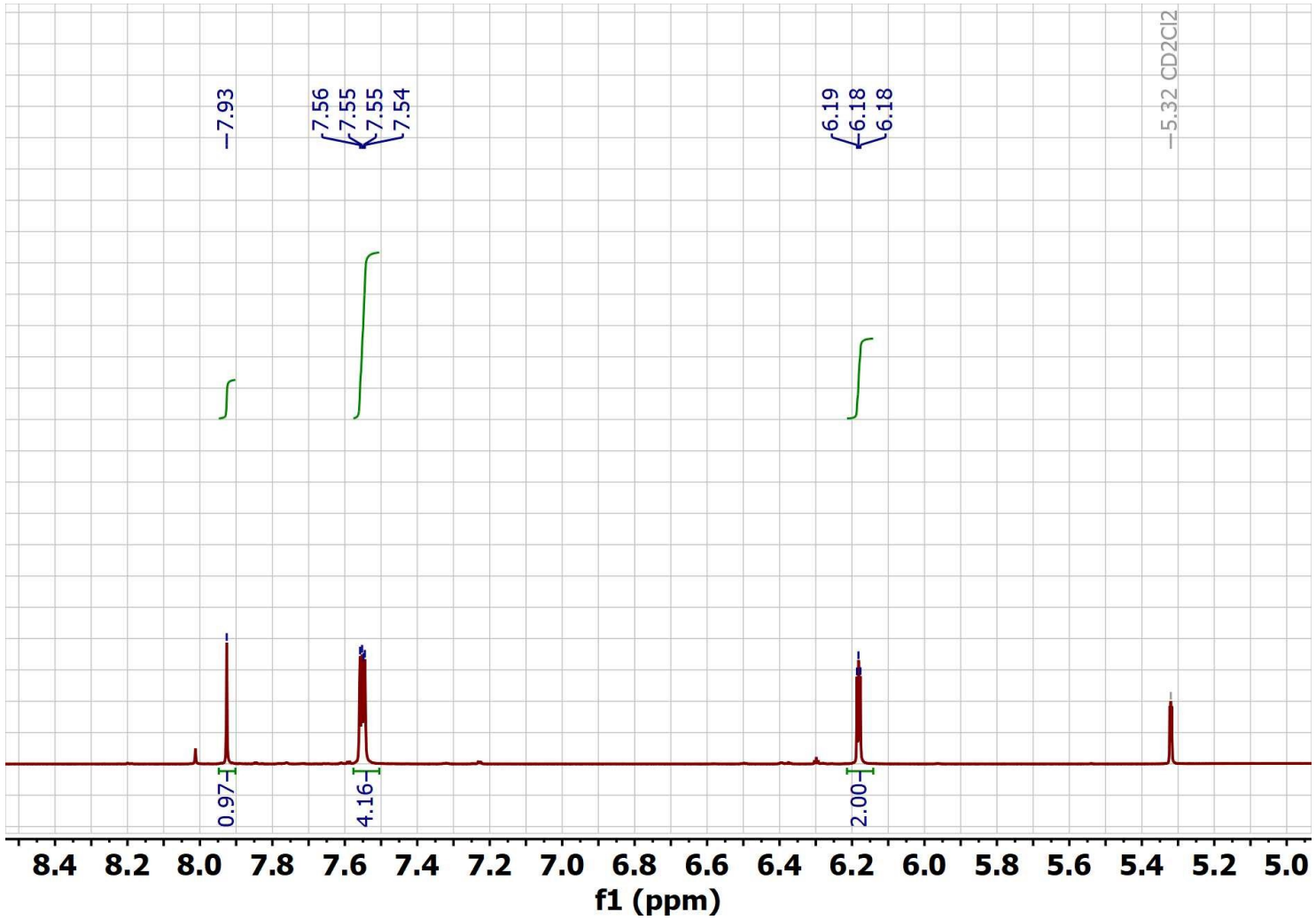

Figure S4: ^{13}C NMR spectrum (aromatic region) of $^{n}Bu_4NL^1$ in CD_2Cl_2.

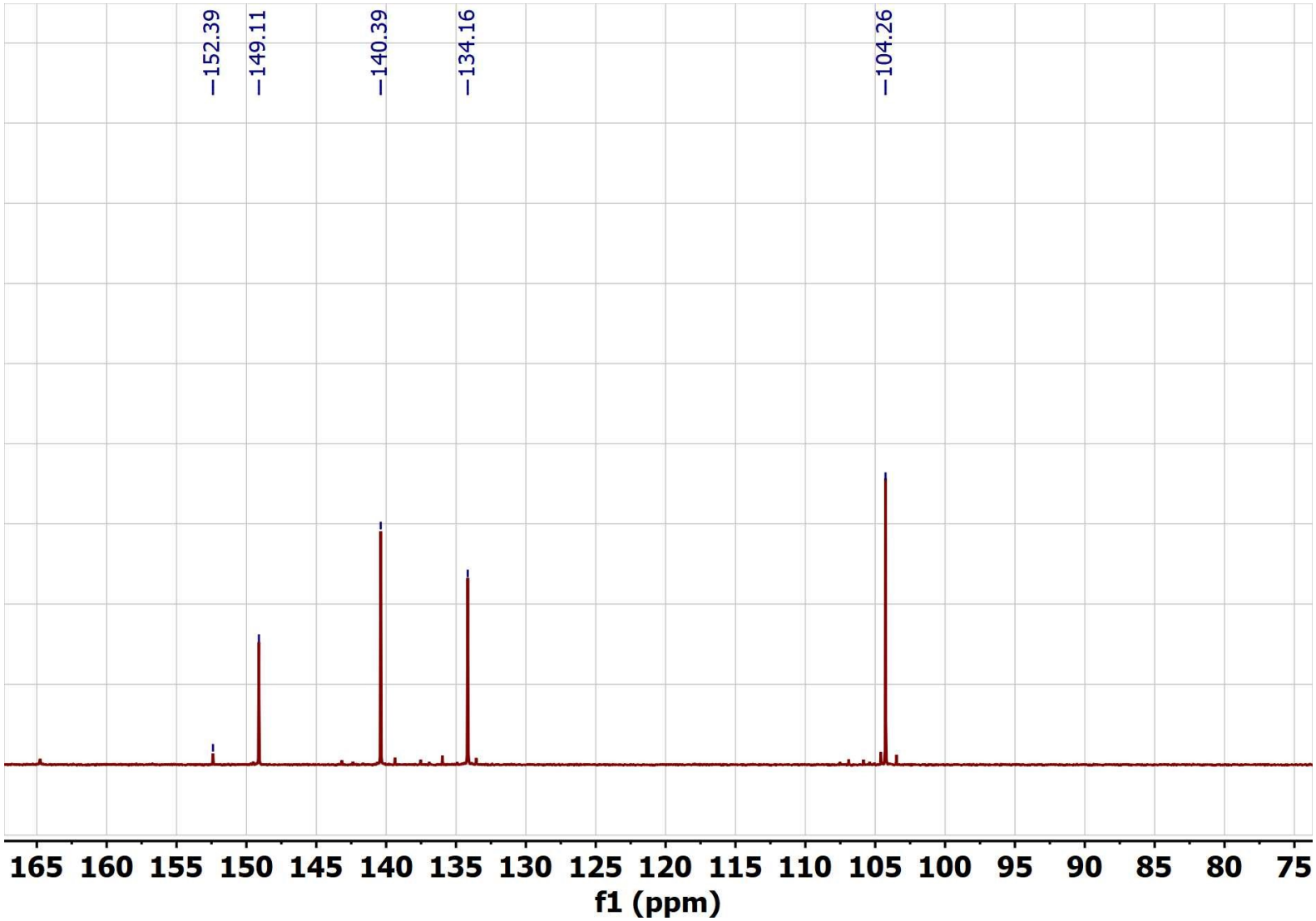

Figure S5: ^{11}B NMR spectrum of $^{n}Bu_4NL^1$ in CD_2Cl_2.

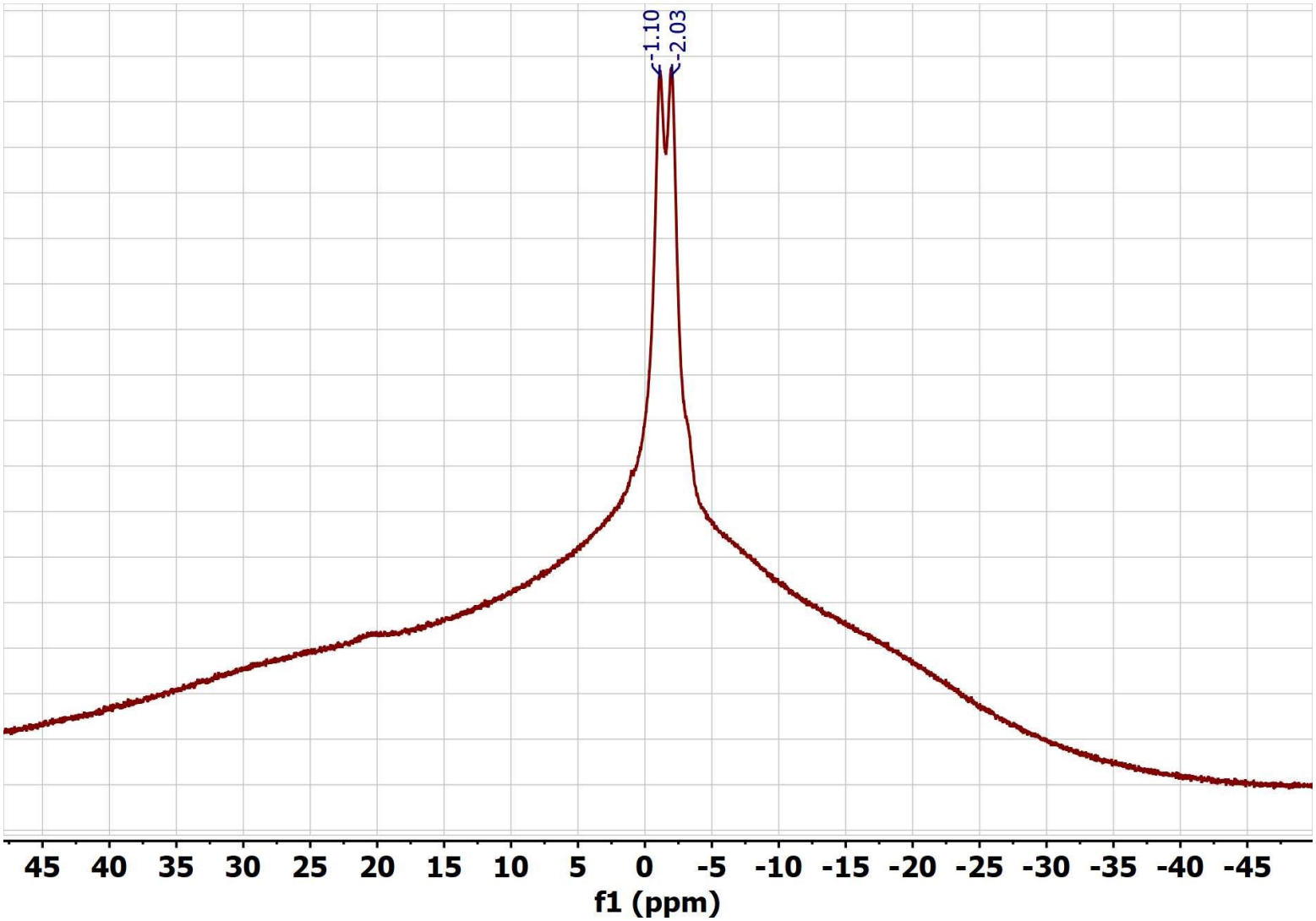

Figure S6: ^{1}H NMR spectrum (aromatic region) of $^{n}Bu_4NL^2$ in CD_2Cl_2.

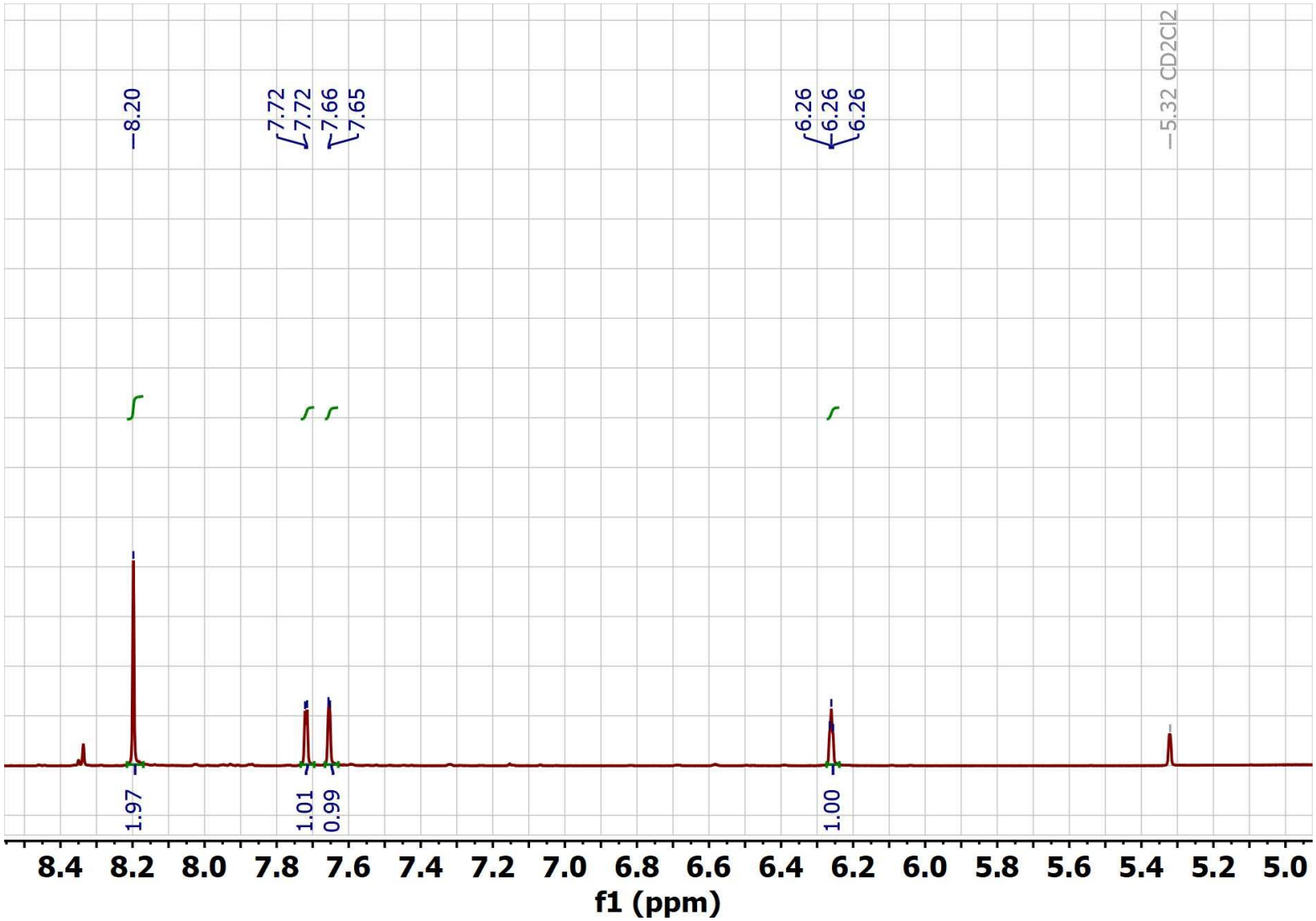

Figure S7: ^{13}C NMR spectrum (aromatic region) of $^{n}Bu_4NL^2$ in CD_2Cl_2.

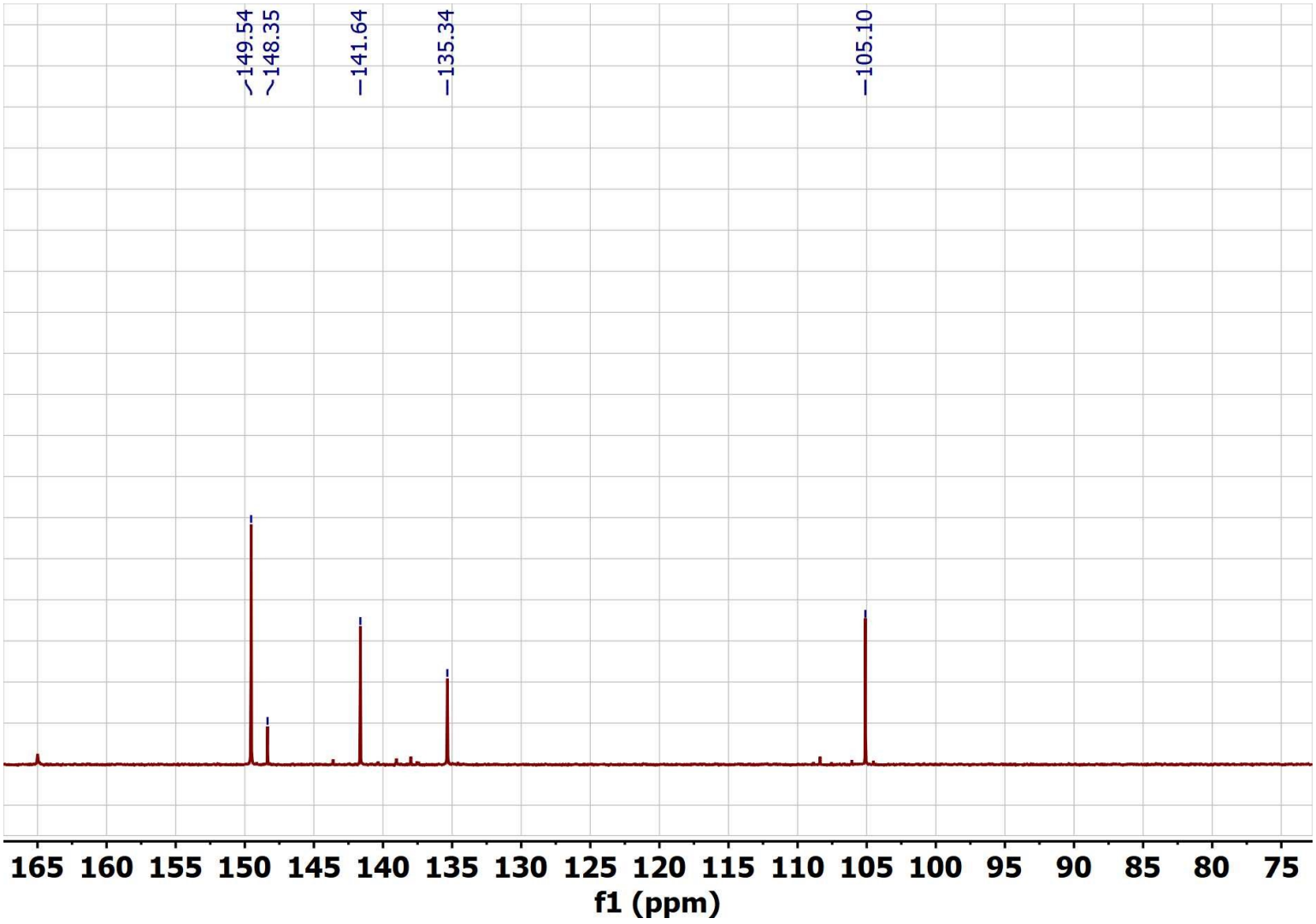

Figure S8: ^{11}B NMR spectrum of $^{n}Bu_4NL^2$ in CD_2Cl_2.

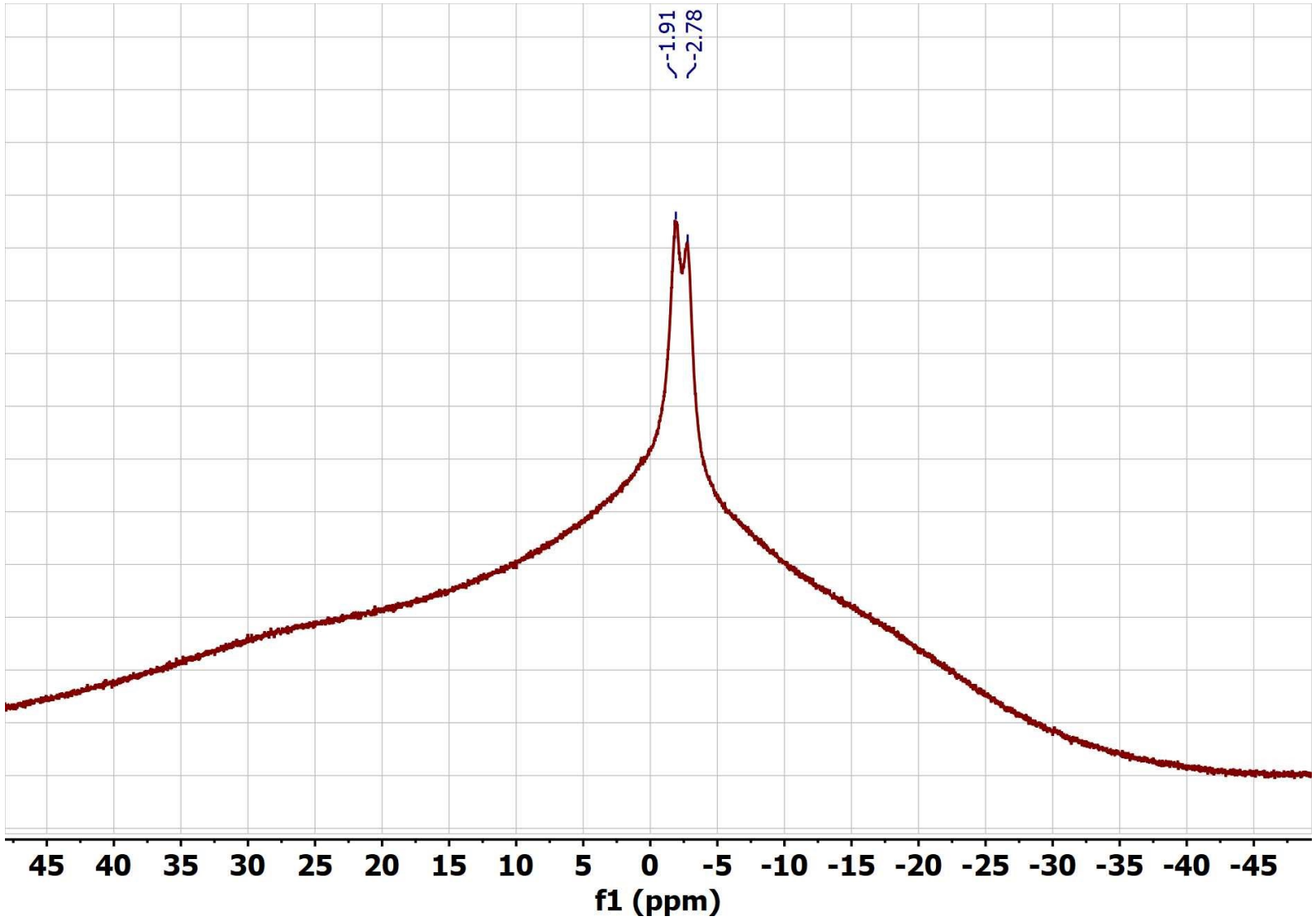

Figure S9: ^{1}H NMR spectrum (aromatic region) of $^{n}Bu_4NL^3$ in CD_2Cl_2.

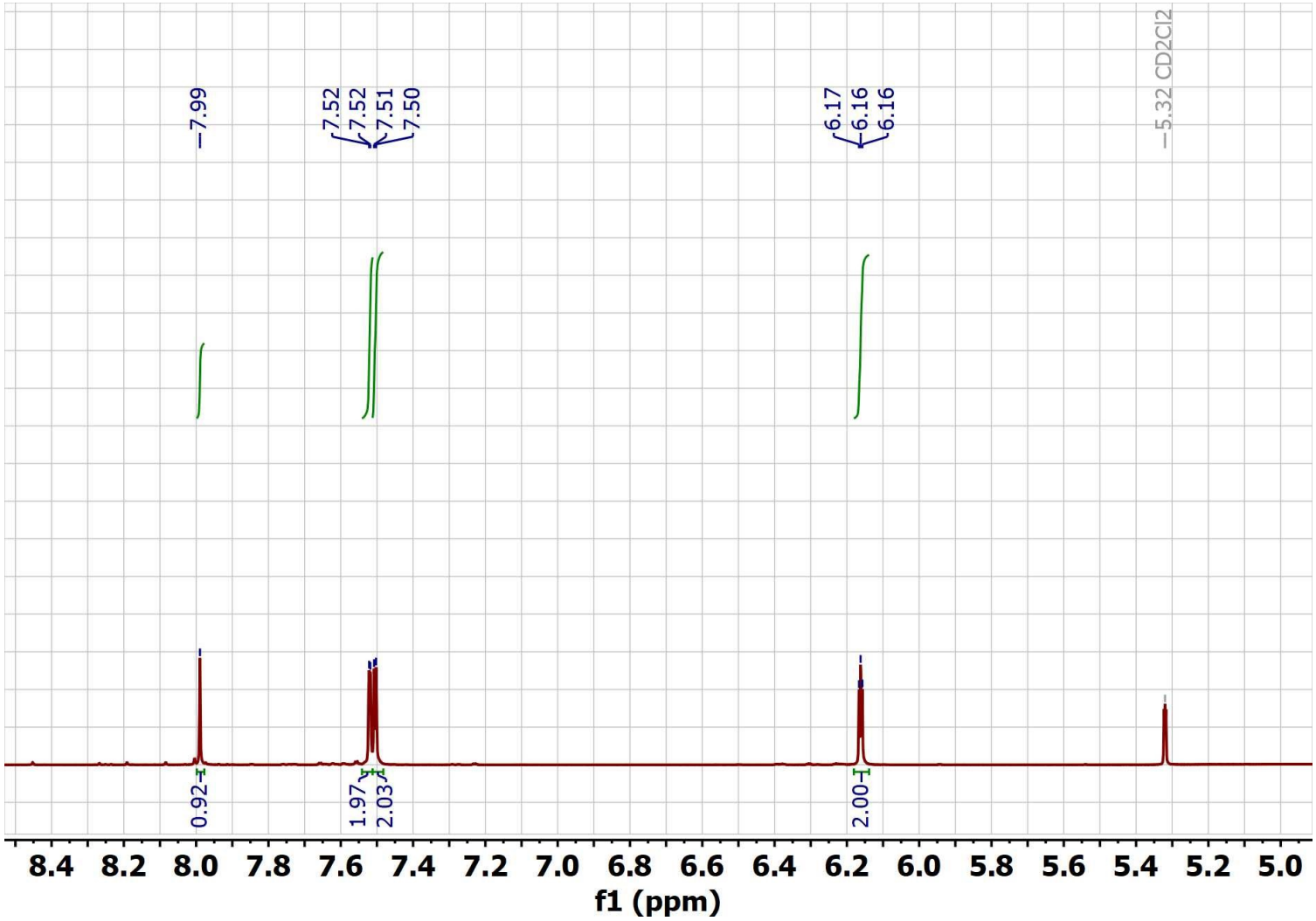

Figure S10: ^{13}C NMR spectrum (aromatic region) of $^{n}Bu_4NL^3$ in CD_2Cl_2.

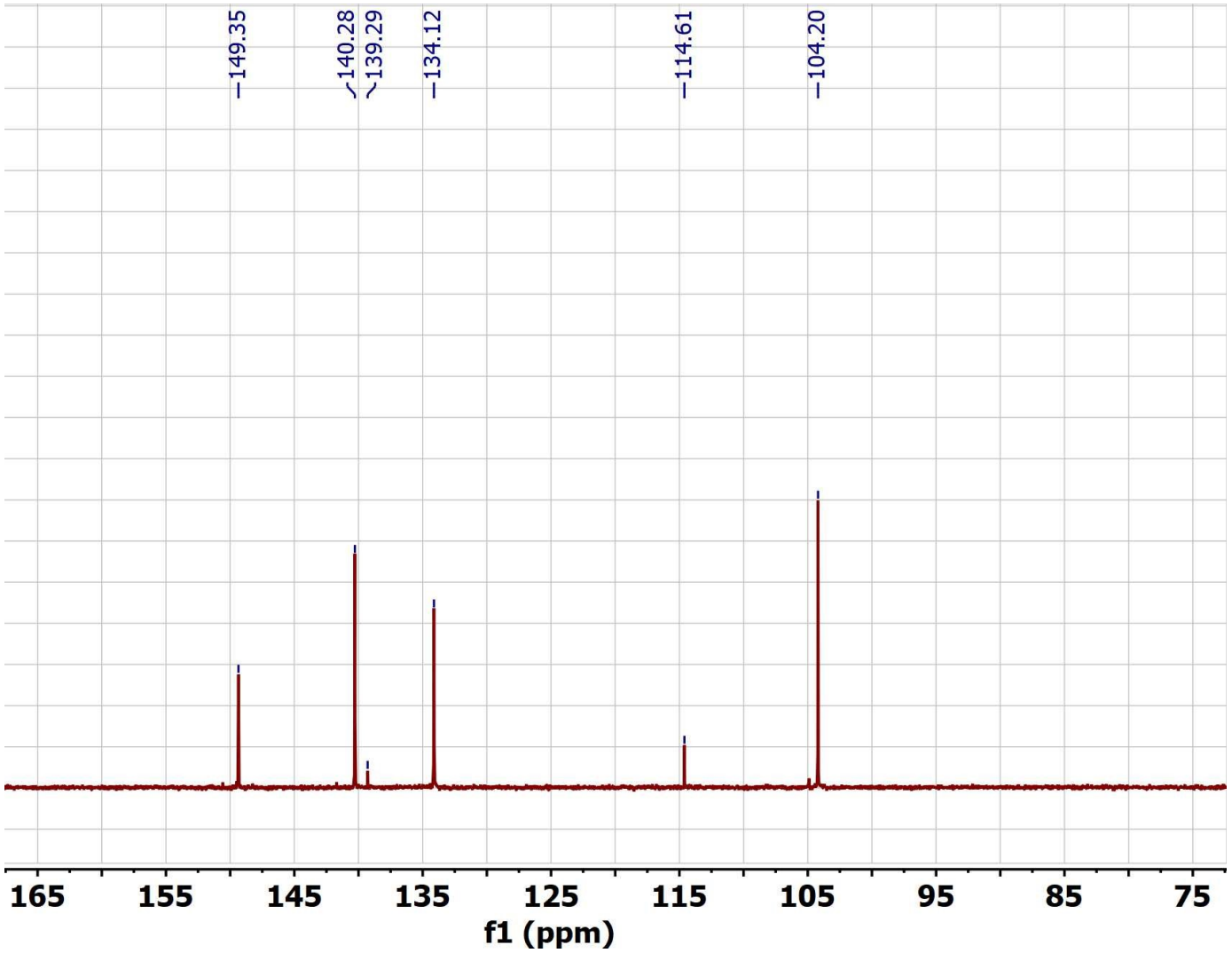

Figure S11: ^{11}B NMR spectrum of $^{n}Bu_4NL^3$ in CD_2Cl_2.

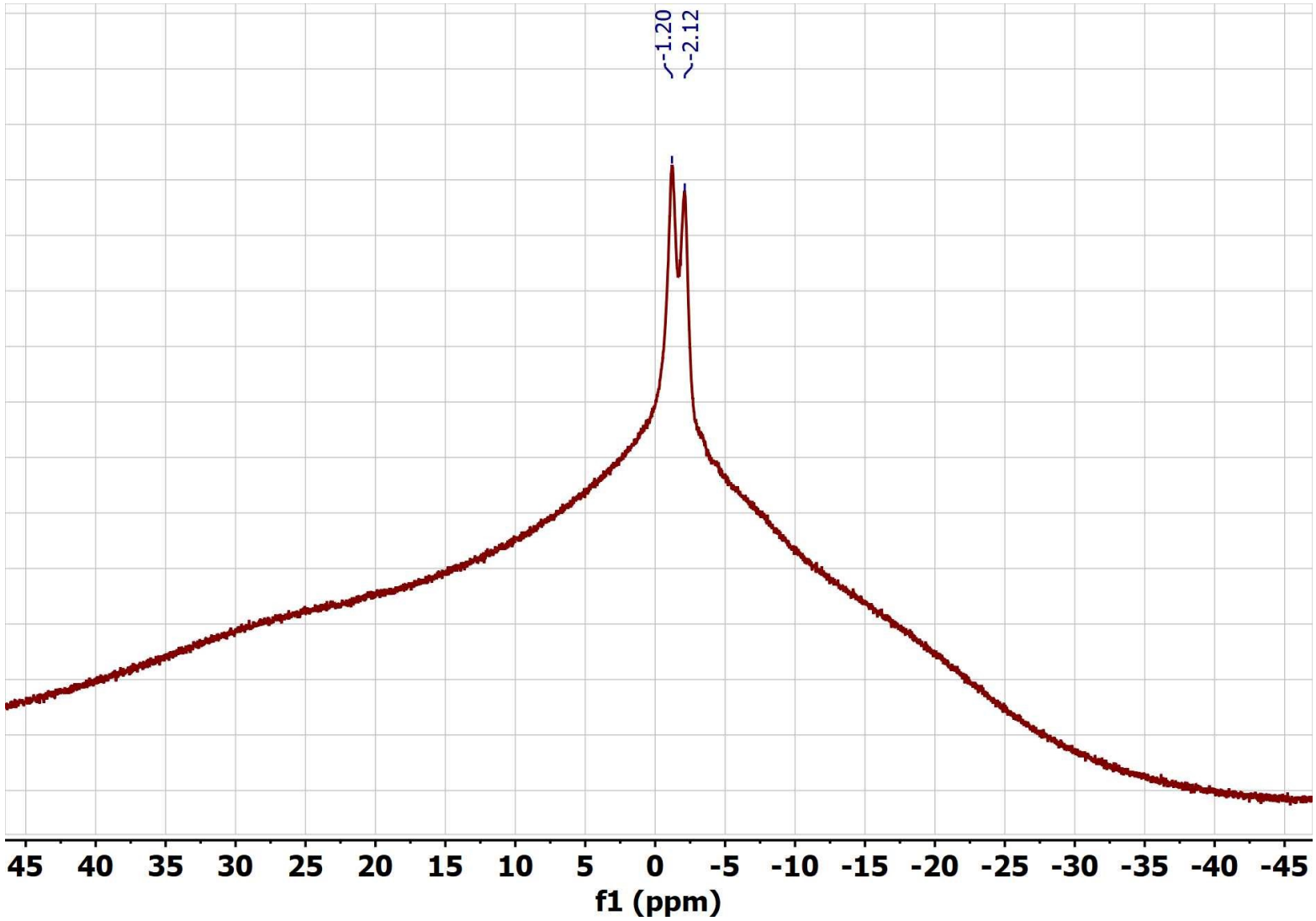

Figure S12: ^{1}H NMR spectrum (aromatic region) of $^{n}Bu_4NL^4$ in CD_2Cl_2.

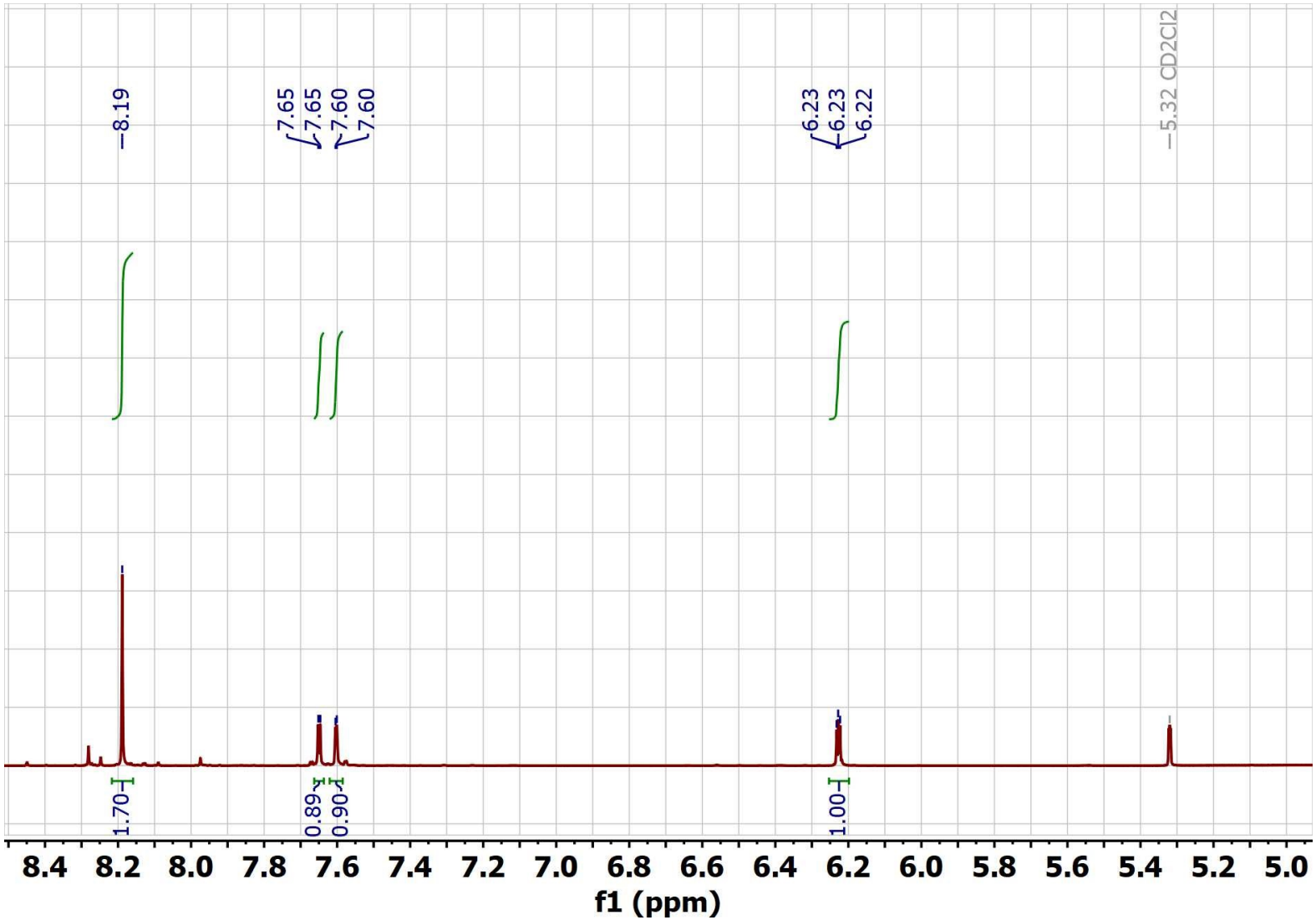

Figure S13: ^{13}C NMR spectrum (aromatic region) of $^{n}Bu_4NL^4$ in CD_2Cl_2.

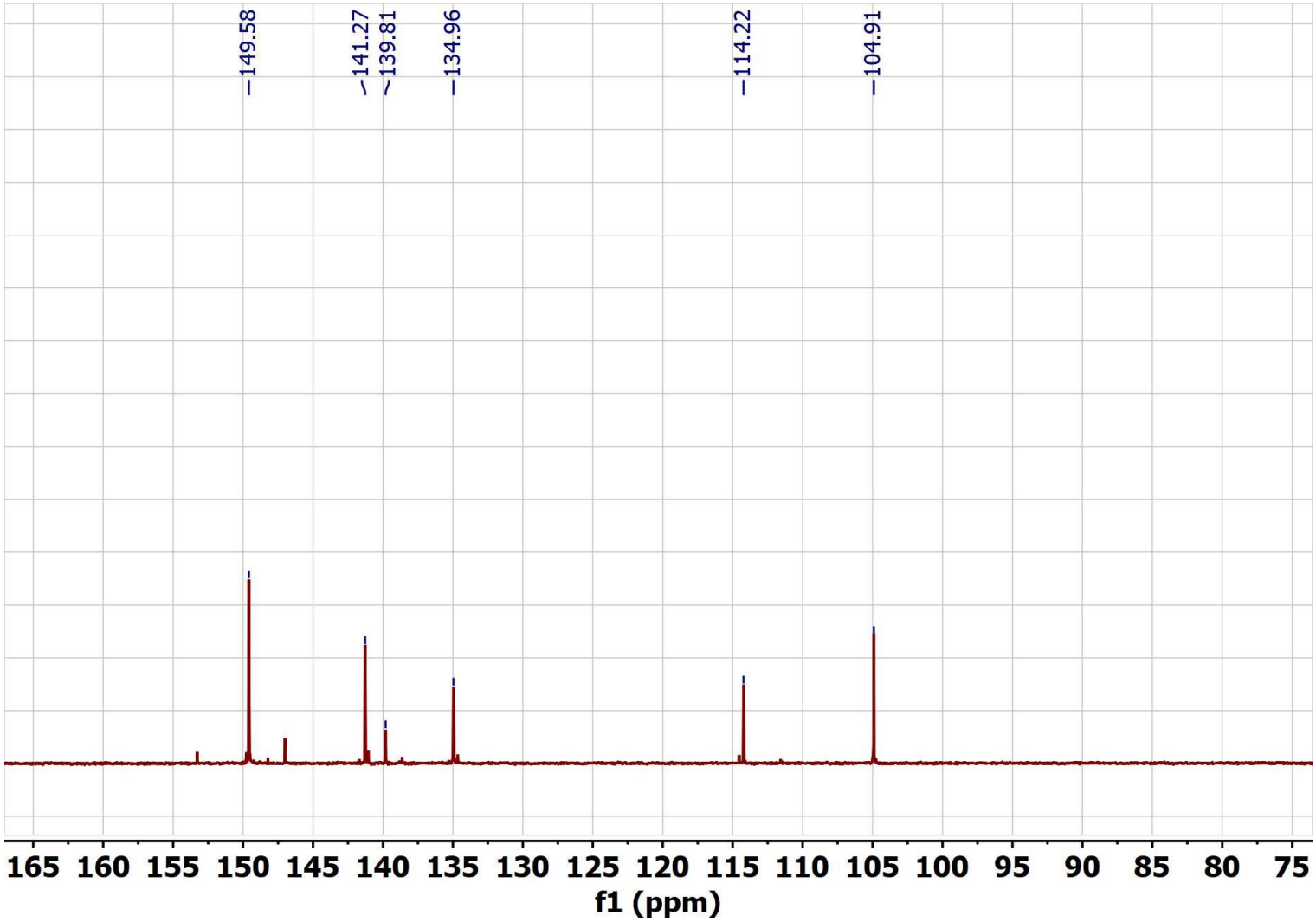

Figure S14: ^{11}B NMR spectrum of $^{n}Bu_4NL^4$ in CD_2Cl_2.

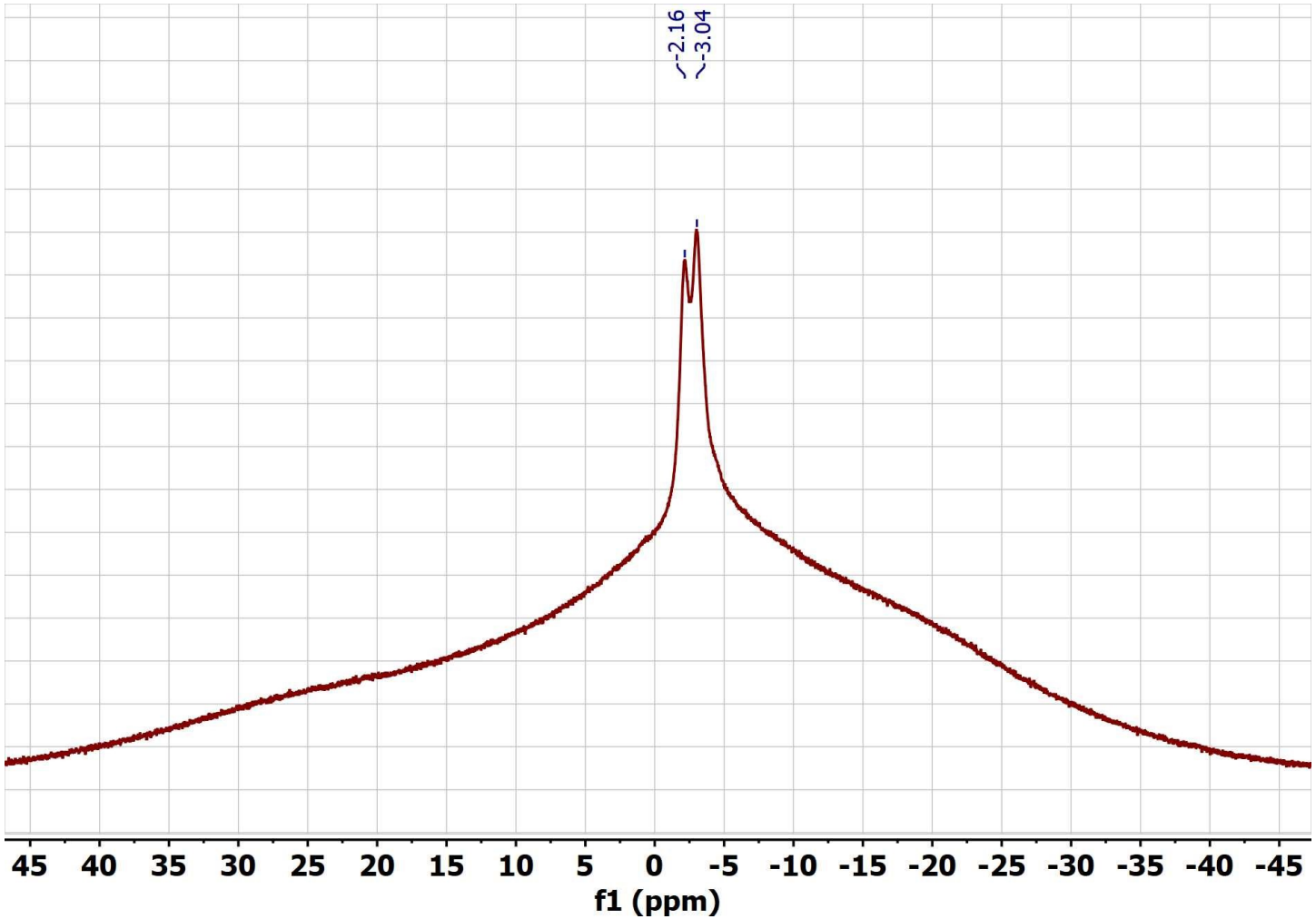

Figure S15: IR spectrum of $^{n}Bu_4NL^1$.

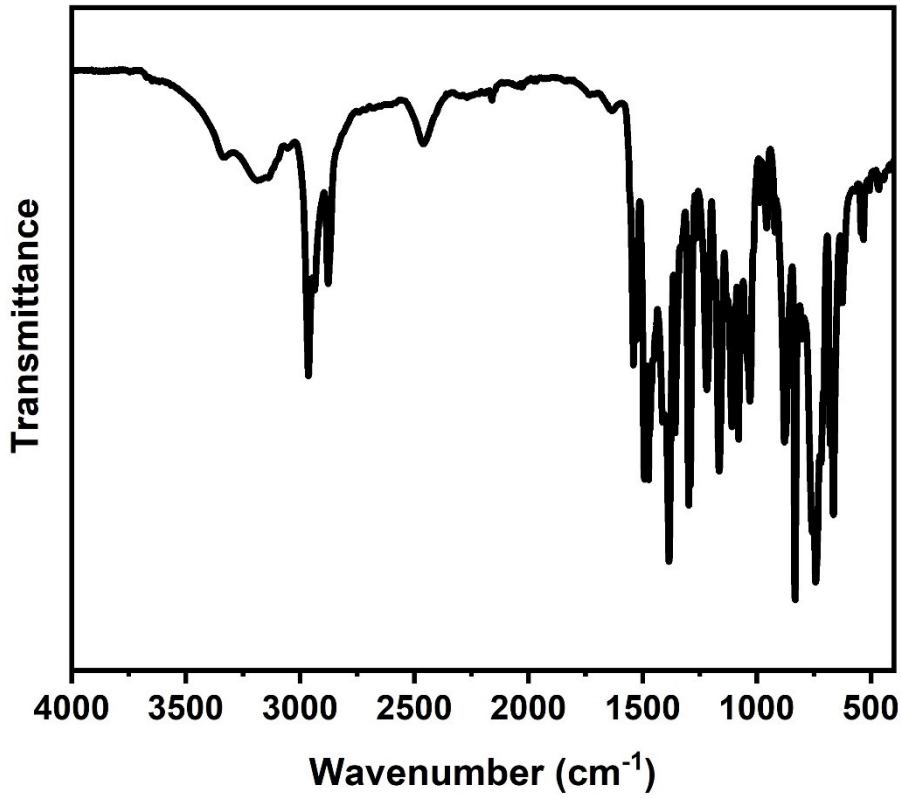

Figure S16: IR spectrum of $^{n}Bu_4NL^2$.

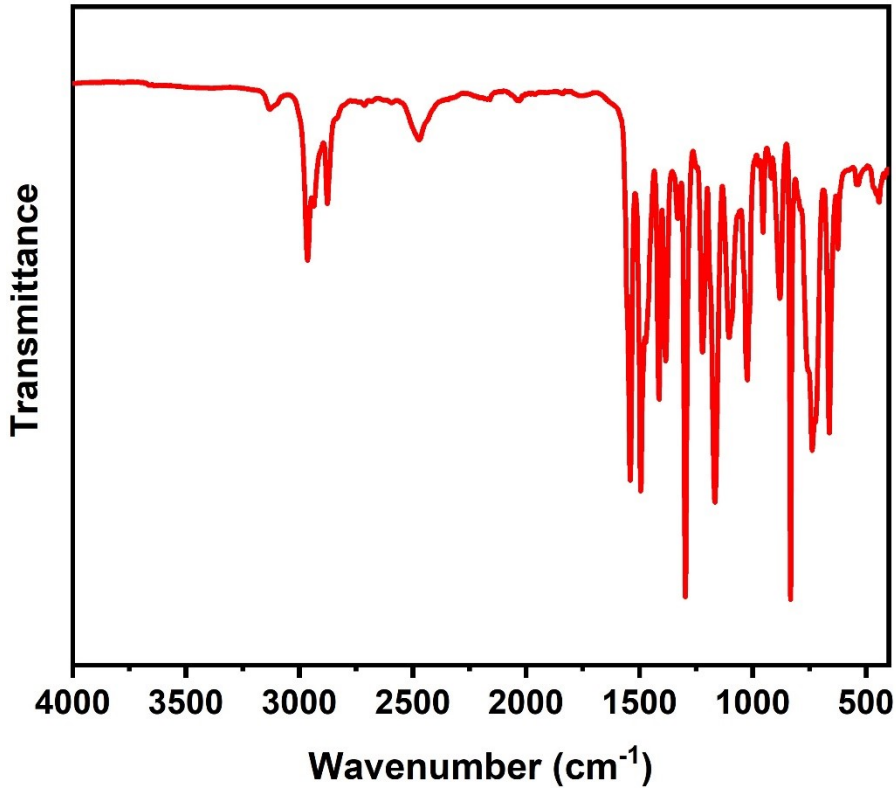

Figure S17: IR spectrum of $^{n}Bu_4NL^3$.

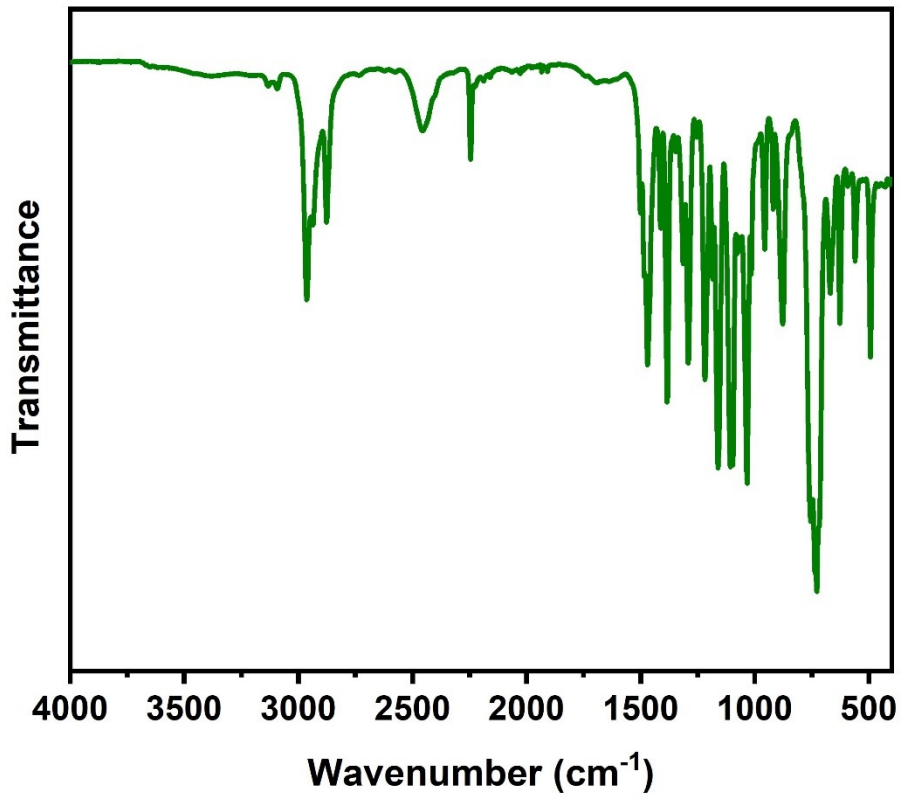

Figure S18: IR spectrum of $^{n}Bu_4NL^4$.

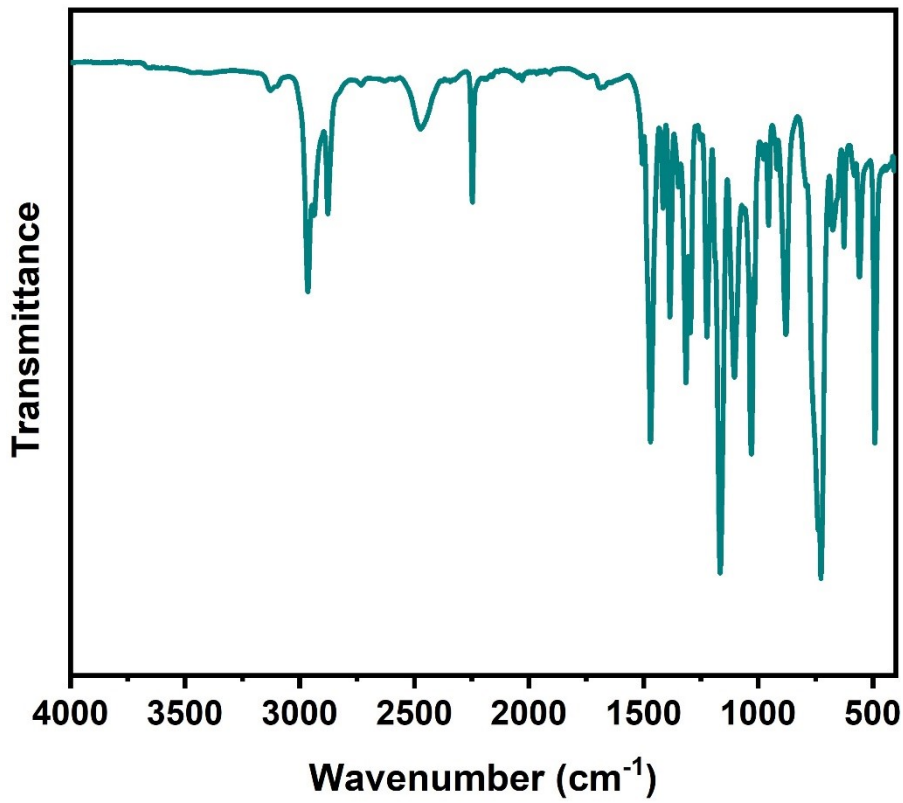

Figure S19: IR spectrum of complex **1**.

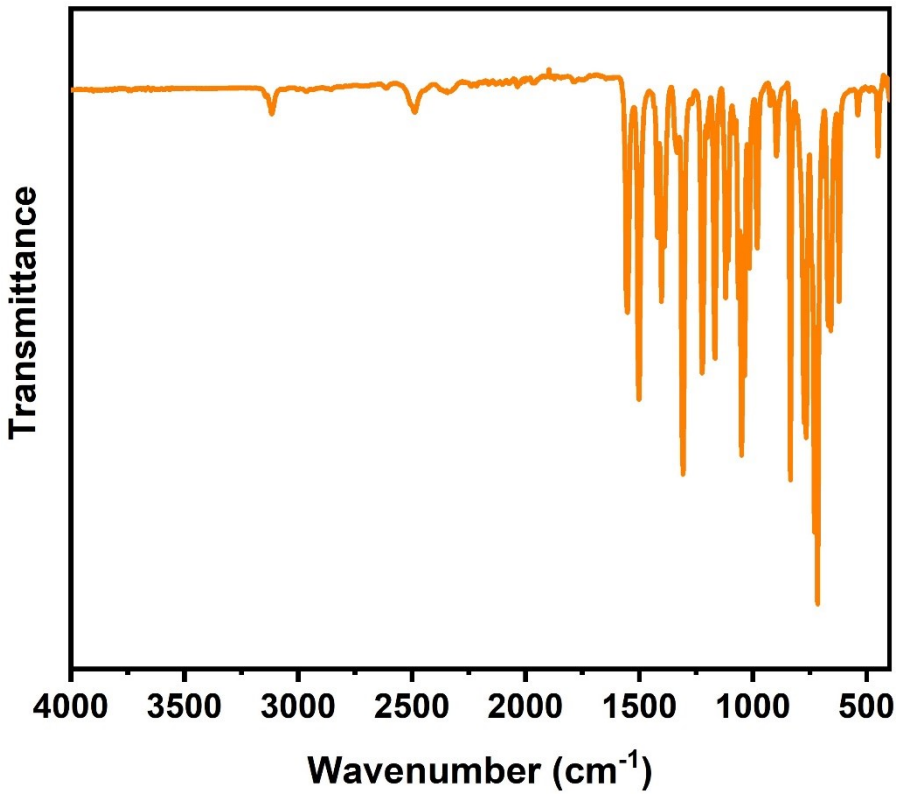

Figure S20: IR spectrum of complex **2**.

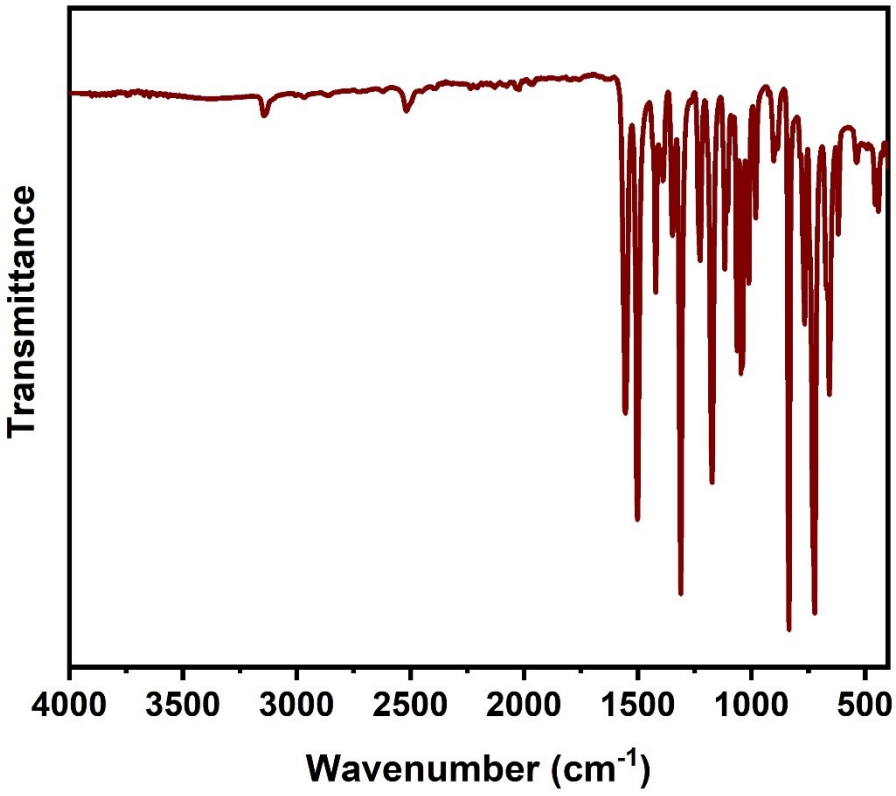

Figure S21: IR spectrum of complex **3**.

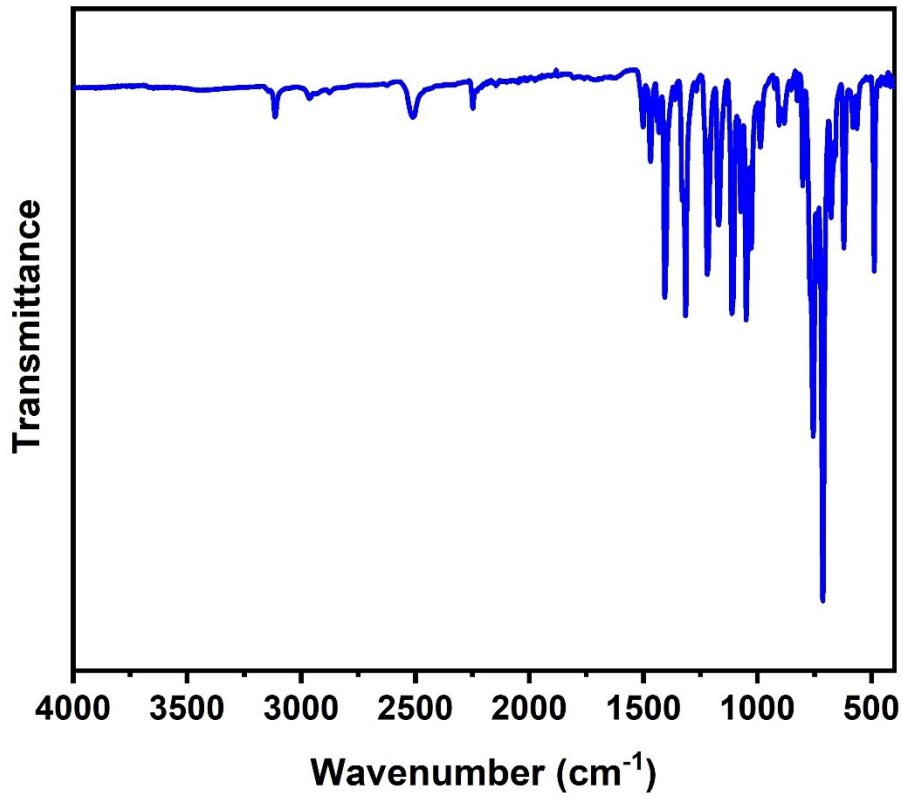

Figure S22: IR spectrum of complex **4**.

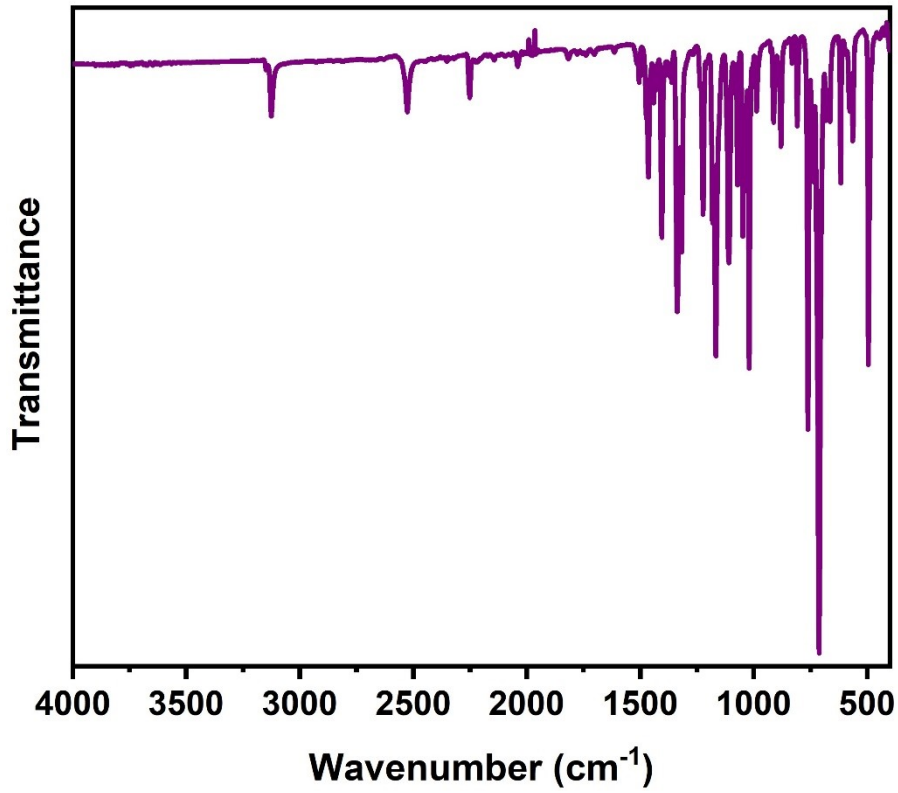

Figure S23: IR spectrum of complex **5**.

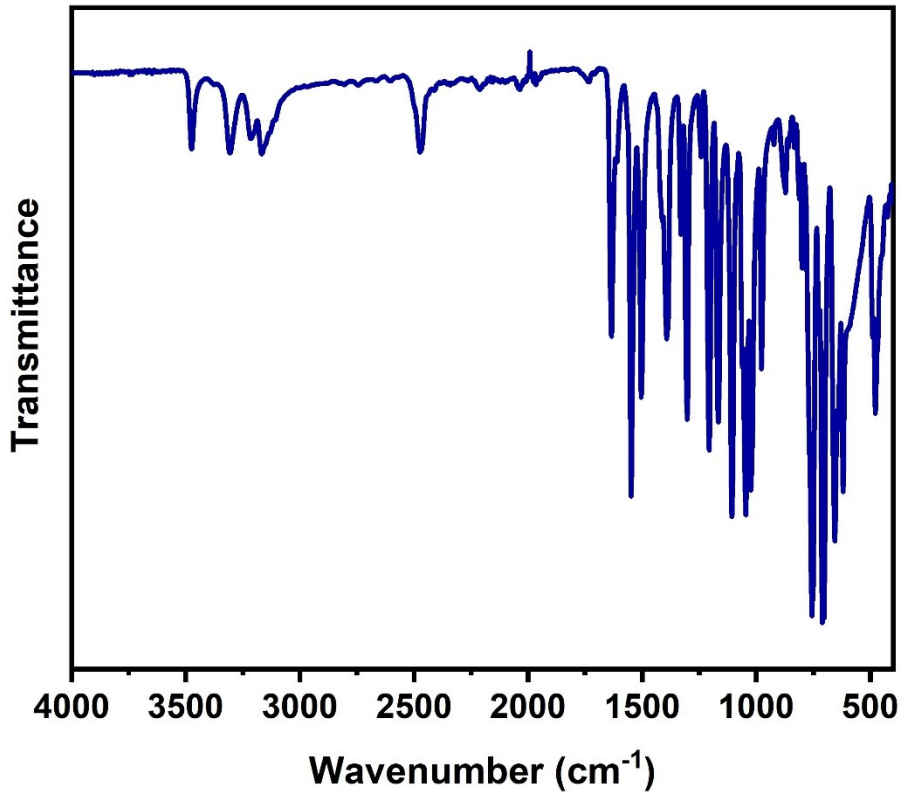

Figure S24: IR spectrum of complex **6**.

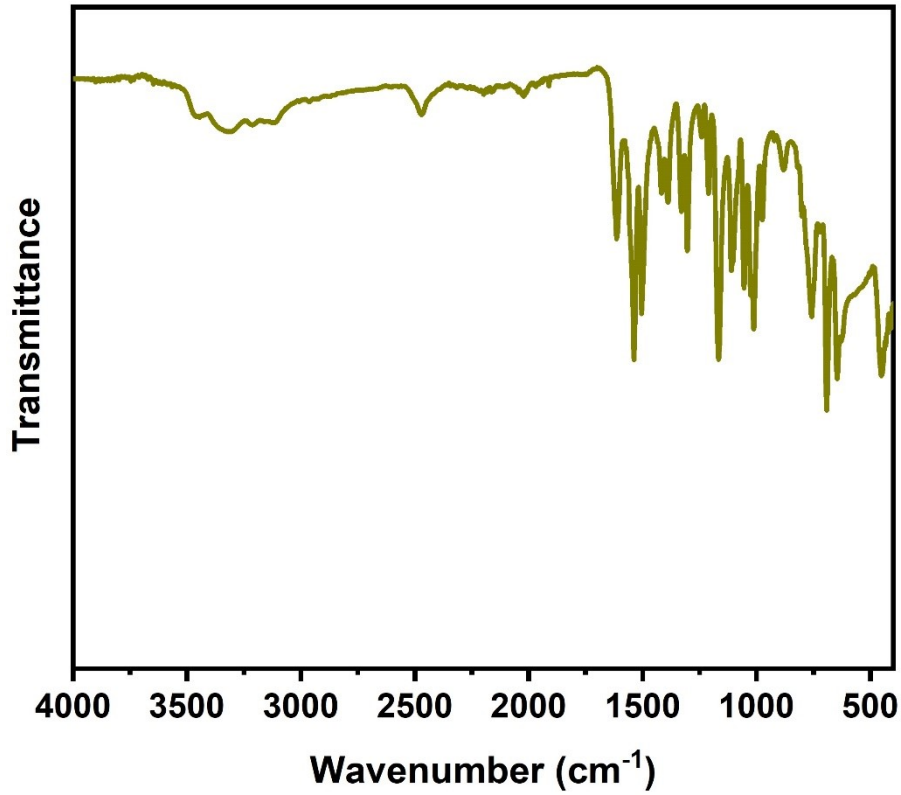

Table S1: Crystal data and structure refinement of **^{n}Bu$_4$NL^1** and complexes **3** and **5** (at 100 K only).

Compound	**^{n}Bu$_4$NL^1**	**3**(*trans*)	**3** (*cis*)·CH_2Cl_2	**5**
Formula weight	501.49	533.90	618.84	509.88
Temperature (K)	173	100	100	100
Space group	$P2_1/n$	$C2/c$	$P2_1/n$	$P2_1/n$
a (Å)	11.9642(1)	9.6251(18)	7.4188(2)	10.364(3)
b (Å)	15.7273(1)	18.494(3)	23.3314(7)	16.490(4)
c (Å)	15.0760(2)	13.335(3)	15.4739(3)	12.598(3)
α, (°)	90	90	90	90
β, (°)	92.122(1)	91.540(6)	101.793(2)	95.789(8)
γ, (°)	90	90	90	90
Cell volume, (Å^3)	2834.82(5)	2372.9(8)	2621.86(12)	2142.1(10)
Z	4	4	4	4
ρ_{calc}(g/cm^3)	1.175	1.494	1.568	1.581
μ (mm^{-1})	0.62	0.68	6.87	0.75
Reflections collected/unique	89937/5001	34154/3978	21400/4449	58852/4388
GoF	1.05	0.85	1.11	0.99
Final *R* indices [$I>2\sigma(I)$]	R_1=0.041, wR_2=0.117	R_1=0.037, wR_2=0.121	R_1=0.076, wR_2=0.214	R_1=0.037, wR_2=0.101

Table S2: Selected geometric parameters for compound **3** (both *trans*- and *cis*-isomers) at 100 K.

Compound			
3 (*trans*)		**3** (*cis*)·CH_2Cl_2	
Fe—N	**Distance (Å)**	**Fe—N**	**Distance (Å)**
Fe1—N4^i	1.9836(14)	Fe1—N12	1.963(4)
Fe1—N2^i	1.9820(15)	Fe1—N14	1.964(4)
Fe1—N6^i	1.9618(14)	Fe1—N6	1.969(4)
Fe1—N6	1.9618(14)	Fe1—N4	1.971(4)
Fe1—N2	1.9820(15)	Fe1—N2	1.972(5)
Fe1—N4	1.9836(14)	Fe1—N10	1.973(4)
N—Fe—N	**Angle (°)**	**N—Fe—N**	**Angle (°)**
N4^i—Fe1—N2^i	89.24(6)	N6—Fe1—N10	90.35(17)
N4^i—Fe1—N6	91.96(6)	N4—Fe1—N10	179.03(18)
N2^i—Fe1—N6	92.21(6)	N2—Fe1—N10	91.04(17)
N4^i—Fe1—N6^i	88.04(6)	N12—Fe1—N14	87.87(18)
N2^i—Fe1—N6^i	87.79(6)	N12—Fe1—N6	177.69(17)
N6^i—Fe1—N6	179.99	N14—Fe1—N6	90.50(18)
N4^i—Fe1—N2	90.76(6)	N12—Fe1—N4	91.58(17)
N2^i—Fe1—N2	179.99	N14—Fe1—N4	90.74(17)
N6—Fe1—N2	87.79(6)	N6—Fe1—N4	90.08(17)
N6^i—Fe1—N2	92.21(6)	N12—Fe1—N2	93.67(19)
N4^i—Fe1—N4	179.99	N14—Fe1—N2	178.10(17)
N2^i—Fe1—N4	90.76(6)	N6—Fe1—N2	88.00(18)
N6—Fe1—N4	88.04(6)	N4—Fe1—N2	88.10(17)
N6^i—Fe1—N4	91.96(6)	N12—Fe1—N10	88.02(17)
N2—Fe1—N4	89.24(6)	N14—Fe1—N10	90.13(17)

Table S3: Unit cell parameters of **5** at selected temperatures.

Parameter	Temperature (K)			
	100	**293**	**320**	**393**
a (Å)	10.364(3)	10.547(3)	10.5951(7)	10.6457(2)
b (Å)	16.490(4)	16.596(4)	16.5995(9)	16.6839(5)
c (Å)	12.598(3)	12.943(4)	12.9503(8)	13.0720(3)
β, (°)	95.789(8)	95.213(10)	94.867(6)	94.662(2)
Cell volume, (Å^3)	2142.1(10)	2256.1(11)	2269.4(2)	2314.06(10)

Table S4: Selected structural parameters for **5** at selected temperatures.

	Temperature (K)			
	100	**293**	**320**	**393**
Distance (Å)				
Fe1—N6	1.9797(19)	2.080(2)	2.103(3)	2.1268(18)
Fe1—N14	1.9772(19)	2.082(2)	2.105(3)	2.1315(19)
Fe1—N10	1.988(2)	2.117(2)	2.130(3)	2.165(2)
Fe1—N2	1.986(2)	2.107(3)	2.132(3)	2.1668(19)
Fe1—N4	1.995(2)	2.134(2)	2.154(3)	2.178(2)
Fe1—N12	1.999(2)	2.120(3)	2.153(3)	2.1868(19)
Angle (°)				
N6—Fe1—N14	179.13(8)	179.37(9)	179.11(12)	178.85(8)
N6—Fe1—N10	91.79(8)	94.01(9)	94.52(12)	94.98(7)
N14—Fe1—N10	87.90(8)	86.61(9)	86.35(12)	86.08(8)
N6—Fe1—N2	87.83(8)	86.23(9)	85.88(12)	85.42(8)
N14—Fe1—N2	91.36(8)	93.80(9)	94.30(12)	95.02(8)
N10—Fe1—N2	89.70(8)	91.33(9)	91.61(12)	92.12(8)
N6—Fe1—N4	89.27(8)	87.47(9)	87.14(11)	86.84(7)
N14—Fe1—N4	91.01(8)	91.91(9)	92.00(12)	92.13(8)
N10—Fe1—N4	178.00(8)	177.29(9)	177.09(12)	177.10(8)
N2—Fe1—N4	88.65(8)	86.50 (9)	86.13(12)	85.76(8)
N6—Fe1—N12	91.71(8)	92.57(9)	92.74(11)	93.07(7)
N14—Fe1—N12	89.09(8)	87.42(9)	87.11(12)	86.54(8)
N10—Fe1—N12	88.83(8)	86.67(9)	86.03(12)	85.66(8)
N2—Fe1—N12	178.44(8)	177.59(9)	177.17(12)	177.20(8)
N4—Fe1—N12	92.83(8)	95.54(9)	96.28 (12)	96.51(8)

Figure S25. Simulated powder pattern from the respective single crystal XRD data (dark grey line) and experimental PXRD pattern (red line) of **5**.

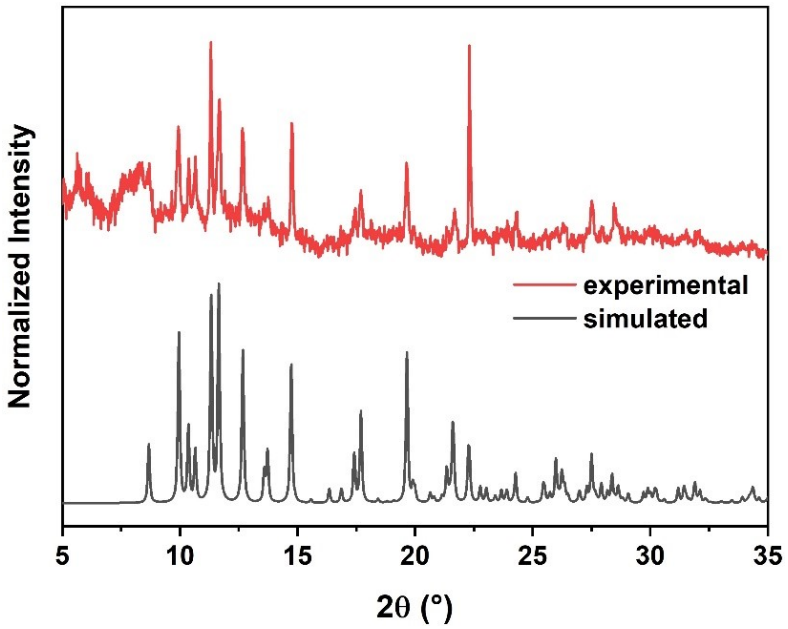

Figure S26. Simulated powder XRD patterns for the *cis*- and *trans*-isomer of **3** and the experimental pattern for the bulk powder of the compound acquired at room temperature.

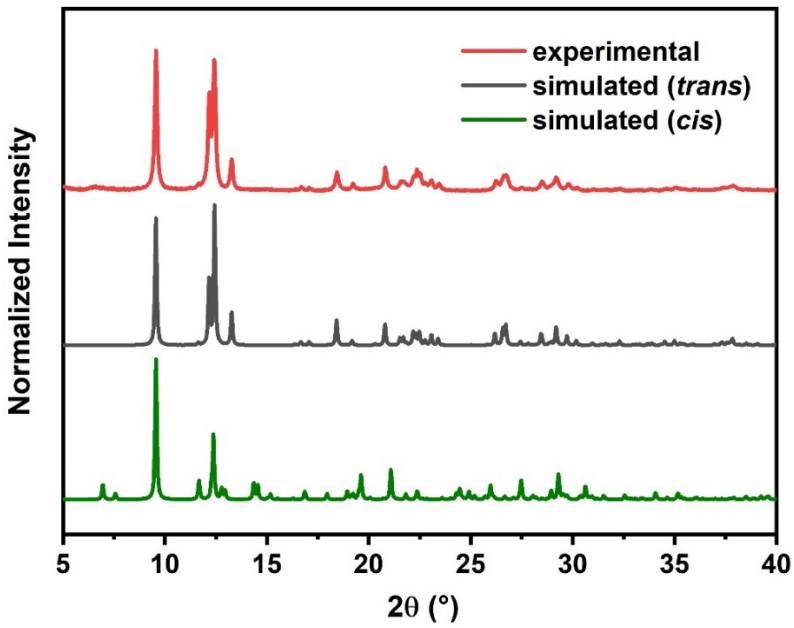

Figure S27: Thermal variation of molar magnetic susceptibility of **5** over three consecutive heating/cooling cycles

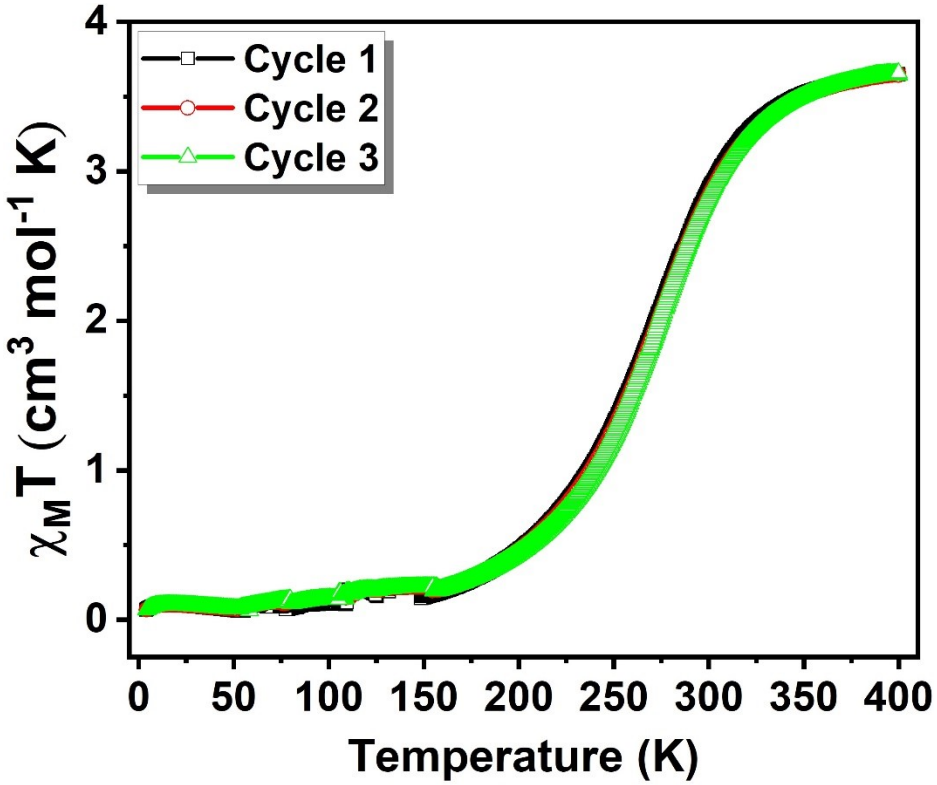

Figure S28. Mössbauer spectra recorded for the bulk powder of **5** at selected temperatures.

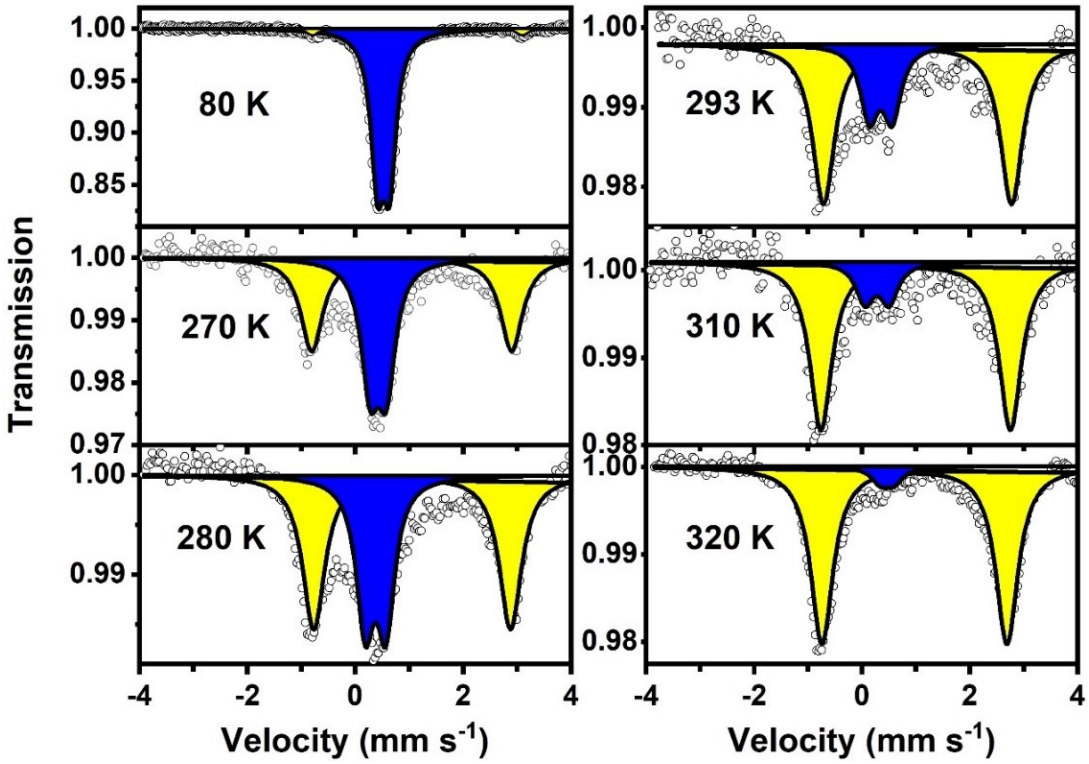

Table S5. Selected parameters determined from the Mössbauer spectra of **5** at selected temperatures. Values in brackets stand for the standard deviation. Fixed values are underlined.

T **(K)**	δ^{HS}/δ^{LS} **(mm·s^{-1})**	$\Delta Eq^{HS}/\Delta Eq^{LS}$ **(mm·s^{-1})**	$HWHM^{HS}/HWHM^{LS}$ **(mm·s^{-1})**	**Acquisition time, (d)**	γ_{HS} **(%)**
80	1.15(2)/0.525(1)	3.89(5)/0.226(2)	0.13(4)/0.146(2)	3	4.0(9)
270	1.05(2)/0.43(1)	3.70(3)/0.30(2)	0.25/0.2	2	50(3)
280	1.057(8)/0.378(9)	3.65(2)/0.38(2)	0.25/0.2	5	58(2)
293	1.03(1)/0.35	3.48(2)/0.42(5)	0.25/0.2	3	74(3)
310	1.00(2)/0.28(8)	3.51(4)/0.45	0.25/0.2	5	84(5)
320	0.975(5)/0.47	3.43(1)/0.25	0.25/0.2	7	94(2)

Figure S29. Correlation of molar magnetic susceptibility thermal variation for **5** (black symbols) and γ_{HS} (red symbols with error bars) extracted from the Mössbauer spectra of the complex acquired at six different temperatures.